

Poroelastic Backus averaging for anisotropic layered fluid- and gas-saturated sediments

Stephan Gelinsky* and Sergei A. Shapiro[†]

ABSTRACT

A homogeneous anisotropic effective-medium model for saturated thinly layered sediments is introduced. It is obtained by averaging over many layers with different poroelastic moduli and different saturating fluids. For a medium consisting of a stack of vertically fractured horizontal layers, this effective medium is orthorhombic. We derive the poroelastic constants that define such media in the long-wavelength limit as well as the effective large-scale permeability tensor. The permeability shows strong anisotropy for large porosity fluctuations.

We observe pronounced effects that do not exist in purely elastic media. At very low frequencies, seismic waves cause interlayer flow of pore fluid across interfaces from more compliant into stiffer layers. For higher frequencies, the layers behave as if they are sealed, and

no fluid flow occurs. The effective-medium velocities of the quasi-compressional waves are higher in the no-flow than in the quasi-static limit. Both are lower than the high-frequency, i.e., ray-theory limit. Partial saturation affects the anisotropy of wave propagation. In the no-flow limit, gas that is accumulated primarily in the stiffer layers reduces the seismic anisotropy; gas that is trapped mainly in layers with a more compliant frame tends to increase the anisotropy. In the quasi-static limit, local flow keeps the anisotropy constant independent of partial saturation effects. For dry rock, no-flow and quasi-static velocities are the same, and the anisotropy caused by layering is controlled only by fluctuations of the layer shear moduli. If the shear stiffness of all layers is the same and only the compressive stiffness or saturation varies, only the ray-theory velocity exhibits anisotropy.

INTRODUCTION

Both reservoir rocks and their overburden often consist of thinly layered sediments. These thin layers can be detected and investigated by ultrasonic core measurements, with sonic logs, and by means of other borehole geophysical methods (Dewan, 1983; Sams, 1995). Properties of single layers, such as permeability and fluid saturation, that are important to delineate a pay zone thus can be determined. If more global information about the reservoir's extension, fluid content, and continuity is needed, seismic waves with longer wavelengths are applied. The wavelength ranges from (approximately) millimeters for ultrasonics to centimeters for sonic logs and up to many meters for vertical seismic profiles (VSP) (1–10 m) and surface seismic investigations (10–100 m). With a wavelength much longer than the layer thicknesses, a single layer cannot be resolved. However, fluctuations of the poroelastic constants, of the density, and of the fluid saturation from layer to layer and their

correlations affect the seismic wavefield and thus the recorded signal.

Wave propagation in fluid-saturated media is commonly described by the Biot theory (Biot, 1956a, 1956b, 1962; Frenkel, 1944). This theory predicts frequency-dependent velocities for two kinds of compressional waves and for shear waves in porous, fluid-saturated rock. The displacements of the solid and fluid phases are coupled. Dissipation is caused by the global flow, which is the relative motion of both continuous phases. Biot theory is an effective-medium theory in the sense that it replaces a medium that is microscopically inhomogeneous (porous) with a homogeneous effective medium. The effective Biot parameters can be derived exactly from the microstructure. An overview is given in Bourbie et al. (1987). To model heterogeneous, layered, saturated porous rock, we apply Biot theory in two ways. First, we describe each homogeneous layer by Biot theory. Second, we parameterize the homogeneous, anisotropic effective medium that replaces the

Manuscript received by the Editor April 29, 1996; revised manuscript received January 2, 1997.

*Formerly Geophysical Institute, Karlsruhe University, Hertzstrasse 16, D-76187 Karlsruhe, Germany; presently Western Atlas Logging Services, 10201 Westheimer, Houston, Texas 77042. E-mail: stephan.gelinsky@wail.com.

[†]Geophysical Institute, Karlsruhe University, Hertzstrasse 16, D-76187 Karlsruhe, Germany. E-mail: sergei@gpiwap2.physik.uni-karlsruhe.de.

© 1997 Society of Exploration Geophysicists. All rights reserved.

stack of layers in the long-wavelength limit in terms of Biot theory.

Heterogeneous, poroelastic media are characterized by several critical frequencies, all separating low- and high-frequency regimes with respect to different physical mechanisms. Upscaling means transforming results that were measured or modeled in one frequency range to a lower one. For example, seismic velocities measured at core samples can be upscaled to predict sonic log velocities. The first basic scale is defined by the ratio between the wavelength λ of an incident wave and a typical length d that describes medium heterogeneities. This d may be the average layer thickness, half a period in periodically layered media, or the correlation length of random heterogeneities. If

$$\frac{d}{\lambda} \ll 1, \quad (1)$$

the system is well described by effective-medium theories. In the opposite limit, for $\frac{\lambda}{d} \ll 1$, the wave propagates along a straight ray in each homogeneous layer, and the complete raypath is defined by Fermat's principle. This limiting case is addressed as ray theory throughout this paper. There is a large zone of intermediate values of λ/d at which a transition from effective-medium to ray-theory behavior can be observed if the layer thicknesses increase from some centimeters to many meters or if the seismic wavelength decreases (Marion et al., 1994; Tang and Burns, 1992). In this range, the frequency dependence of seismic wavefield parameters becomes important. Applying the generalized O'Doherty-Anstey formalism for elastic waves, Shapiro and Hubral (1996) found that the anisotropy of the phase velocity even at seismic frequencies can be significantly below the one derived in the static limit (i.e., the Backus averaging for anisotropy). Using surface seismic and borehole information, one can take thin layering into account directly and correct the amplitude-variation-with-offset response of a target zone with a thinly layered elastic overburden for effects caused by the stack of layers (Widmaier et al., 1995, 1996).

The response of poroelastic, fluid-saturated media to seismic excitations is a complicated function of frequency even in the absence of any large-scale heterogeneities. In the quasi-static limit, i.e., for frequencies below a characteristic frequency

ω_0 [defined in equation (2)], the pore fluids are equilibrated perfectly across the interfaces by interlayer flow (also termed squirt and local flow; Gurevich and Lopatnikov, 1995). Above this characteristic frequency, the Biot slow wave exists only within a thin boundary layer near each interface, and the layers behave as if they were isolated. Thus, the effective-medium regime can be divided further into two ranges, separated by the characteristic frequency at which the attenuation length of the Biot slow compressional wave equals the mean characteristic length d ,

$$\omega_0 = \frac{kN}{\eta d^2}. \quad (2)$$

Here, k is permeability; η is viscosity; $N = M(K_d + 4/3\mu_d)/H$; K_d and μ_d are the bulk and shear moduli of the dry rock matrix, respectively; and the poroelastic moduli M and H are defined later [in equations (7) and (9)]. Below this characteristic frequency in the quasi-static limit, the fluid pressure is equilibrated across layer boundaries because of the Biot slow wave that for these frequencies describes diffusive transport (Chandler and Johnson, 1981; Norris, 1993). Above the characteristic frequency ω_0 in the no-flow limit, the layers behave like isolated structures, since the (propagating) Biot slow wave is highly attenuated for these frequencies, so the fluid pressure is no longer equilibrated. We calculated ω_0 for various porous sediments. Its value ranges from a few hertz for thick layers of low permeability to many kilohertz for thin, high-permeability layers. (see Table 1).

Independent of scale effects caused by heterogeneities, velocity dispersion occurs even in macroscopically homogeneous materials (Wang and Nur, 1992; Mukerji and Mavko, 1994). Biot theory predicts a difference between the high- and low-frequency velocities in saturated rocks because the displacements of the solid and fluid phases are coupled. Dissipation is caused by the global flow, which is the relative motion of both continuous phases. Biot defined a critical frequency as

$$\omega_c = \frac{\eta\phi}{k\rho_f}. \quad (3)$$

Here, ϕ is porosity and ρ_f is the fluid density. This critical frequency separates two different regimes. For low frequencies,

Table 1. Rock properties.

Parameter	Unit	Rock 1, Berea ⁽¹⁾	Rock 2, porous rock ⁽²⁾	Rock 3, porous rock ⁽²⁾	Rock 4, weak sandstone ⁽³⁾	Rock 5, coarse sand ⁽³⁾
K_d	10^9 Pa	7.9	12.7	4.3	2.2	0.22
K_g	10^9 Pa	37.9	40.0	40.0	36.0	36.0
μ_d	10^9 Pa	15.8	20.3	8.8	1.0	0.10
ϕ		0.19	0.15	0.17	0.30	0.35
ρ_d	kg/m ³	2146	2252	2200	1855	1723
ρ_g	kg/m ³	2650	2650	2650	2650	2650
k	10^{-12} m ²	0.2	0.1	0.2	1000	1000
$\omega_0/2\pi$ ⁽⁴⁾	Hz	26	17	22	39 900	5400
$\omega_0/2\pi$ ⁽⁵⁾	Hz	425	270	475	1.3×10^6	1.2×10^6
$\omega_c/2\pi$ ⁽⁶⁾	Hz	1.5×10^5	2.4×10^5	1.4×10^5	48	56

⁽¹⁾Norris, 1993.

⁽²⁾Gurevich and Lopatnikov, 1995.

⁽³⁾Turgut and Yamamoto, 1990.

⁽⁴⁾Characteristic frequency as defined in equation (2) for layers of 10-cm thickness and water saturation. For layer thicknesses of 1 cm, ω_0 is 100 times larger.

⁽⁵⁾As in footnote 4, but for layers of 1-cm thickness and gas saturation.

⁽⁶⁾Biot's critical frequency as defined in equation (3). For gas saturation, ω_c is approximately 1.5 times larger.

the fluid motion is dominated by viscosity, whereas for frequencies above ω_c , inertia and tortuosity are more important (Rasolofosaon, 1991). For the materials that we have studied in more detail, we give ω_c in Table 1. For frequencies below ω_c , the velocity can be calculated according to Gassmann's formula (White, 1983). For high frequencies, as in the ray-theory limit, the velocity is slightly higher. Geertsma and Smit (1961) derived a simple expression for the Biot high-frequency limiting P -wave velocity [equation (16)], which we discuss in the section on no-flow limit.

In this paper, we transform Biot's second-order differential equations to a system of first-order differential equations. By averaging over all layers, the heterogeneous medium is replaced by a homogeneous effective medium. Fluctuations of the poroelastic constants from layer to layer lead to anisotropy. In the low-frequency limit, the layered medium behaves like an anisotropic homogeneous effective medium with the z -axis as a symmetry axis. This averaging is a generalization of the Backus averaging technique, originally proposed for elastic media (Backus, 1962; Bruggemann, 1937).

For isotropic layers, the results for the poroelastic moduli are consistent with those given in Norris (1993). Additionally, with the new method, the complete poroelastic tensor is determined and upscaling rules for the permeability tensor are automatically included. Thus, this technique can serve as a basis to study the influence of porosity fluctuations and fluid properties on the propagation of obliquely incident qP , qS_1 , and qS_2 seismic plane waves in a poroelastic, fluid-saturated, fractured, finely layered medium, taking thin layering consistently into account. Such a numerical modeling of wave propagation for poroelastic media with anisotropy caused by an anisotropic dry frame was presented recently in Carcione (1995).

After the introduction of the poroelastic generalization of Backus averaging, basic results for isotropic layers are derived and compared for various limiting cases (quasistatic, no flow, and ray theory). The influence of partial saturation is discussed for different media (see Figures 2 to 8). Next, the scheme is generalized to anisotropic layers (e.g., layers containing shale or aligned fractures). Finally, the behavior of the effective permeability is considered, and permeability anisotropy as a function

of porosity fluctuations is investigated (see Figures 9 and 10). The paper concludes with a discussion of the results.

THEORY

Dynamic equations

Starting points are the second-order Biot (1962) differential equations

$$\frac{\partial}{\partial x_j} \tau_{ij} = \frac{\partial^2}{\partial t^2} (\rho u_i + \rho_f w_i) \tag{4}$$

and

$$-\frac{\partial}{\partial x_i} p_f = \frac{\partial^2}{\partial t^2} (\rho_f u_i + q_{ij} w_j). \tag{5}$$

On the left-hand sides, τ_{ij} and p_f are the elements of the stress tensor and the hydrostatic pressure. For isotropic layers, the stress-strain relations are given later [in equation (10)]. The variables u and w are the displacement of the solid phase and the relative solid-fluid displacement, respectively; the indices i, j denote the Cartesian coordinates; and $\rho = \phi \rho_f + (1 - \phi) \rho_g$ is the density of the saturated composite. Throughout this paper, the index d is used for properties of the dry rock frame, i.e., the matrix; the index g is used for properties related to the grain, i.e., the matrix material; and the index f is used for fluid properties. The permeability enters into the Biot equations through the dissipation term q_{ij} . Permeability and tortuosity are tensors with elements k_{ij} and a_{ij} , respectively. With $\mathbf{r} = \mathbf{k}^{-1}$, the definition of q_{ij} is

$$q_{ij} = i \frac{\eta r_{ij}}{\omega} + \frac{\rho_f a_{ij}}{\phi}. \tag{6}$$

In the isotropic case, $q_{ij} = q \delta_{ij}$, since permeability $k_{ij} = k \delta_{ij}$ and tortuosity $a_{ij} = a \delta_{ij}$. A closer look at the frequency dependence of q explains the definition of Biot's characteristic frequency ω_c as given by equation (3). The tortuosity that is numerically close to unity usually is omitted.

Following Biot, we parameterize each layer by its porosity, permeability, density, several poroelastic constants, and the fluid parameters viscosity, density, and bulk modulus. The tortuosity becomes important only above Biot's critical frequency. The necessary number of parameters depends on the symmetry properties of the layer materials. Isotropic layers are specified by four poroelastic constants and one value of permeability; transversely isotropic (TI) layers are specified by eight poroelastic constants and two values of directional permeability. The specification of poroelastic media requires more constants than does that of elastic media. These are needed because of the existence of an additional fluid phase and its influence on the compressibility of the saturated rock. Biot and Willis (1957) discuss the measurements that are needed to determine all Biot constants by means of jacketed and unjacketed compressibility tests in the laboratory. The number of additional parameters depends on the symmetry of the medium. For isotropic media, the two constants are σ and M ,

$$\begin{aligned} \sigma &= 1 - \frac{K_d}{K_g}, \\ M &= \left[\frac{\phi}{K_f} + \frac{\sigma - \phi}{K_g} \right]^{-1}. \end{aligned} \tag{7}$$

Here, K_g is the grain bulk modulus (the material of the dry frame) and K_f is the fluid bulk modulus. For TI media, three

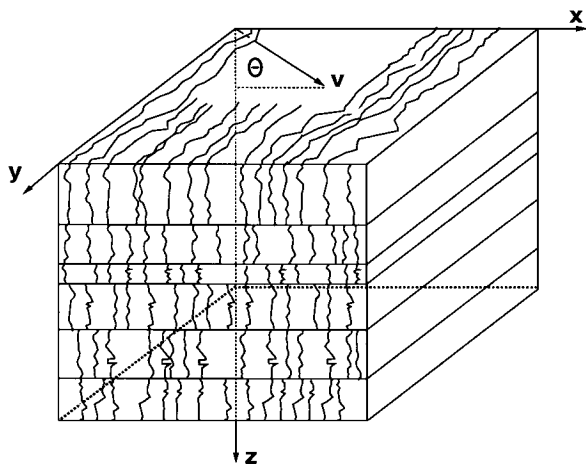


FIG. 1. Vertically fractured and horizontally layered medium. The single layers are TIH, with the x -axis as the symmetry axis. The effective medium is orthorhombic.

additional parameters are required (B_6, B_7, B_8 or P, Q, R); for orthorhombic media, four are required (M_1, M_2, M_3, M). The maximum number of additional poroelastic constants in the most general case of anisotropy is seven; i.e., the medium is characterized by 28 constants.

We study plane-wave propagation in vertically inhomogeneous media. Therefore, we use the following starting point for the displacement of the solid phase \mathbf{u} (and, respectively, for the relative solid-fluid displacement \mathbf{w} and the stresses τ_{ij}):

$$\mathbf{u} = (u_x(z), u_y(z), u_z(z))e^{-i\omega t + ip_x x + ip_y y}. \quad (8)$$

The hydrostatic pressure p_f is treated in a similar way. For isotropic P - and SV -wave problems and those with transverse isotropy and a vertical symmetry axis (TIV), the description can be simplified by setting $p_y, u_y,$ and w_y equal to zero without a loss of generality. To develop the basic concepts, we first discuss isotropic layers and use this simplification. Later, we discuss the more general case of non-TIV anisotropic layers. The saturated P -wave modulus is defined, according to Gassmann, as

$$H = K_d + \frac{4}{3}\mu_d + \sigma^2 M. \quad (9)$$

The (nonzero) stress-strain relations are (the prime denoting the derivative with respect to z)

$$\begin{aligned} \tau_{xx} &= H \nabla \mathbf{u} - 2\mu u'_z + \sigma M \nabla \mathbf{w}, \\ \tau_{yy} &= H \nabla \mathbf{u} - 2\mu \nabla \mathbf{u} + \sigma M \nabla \mathbf{w}, \\ \tau_{zz} &= H \nabla \mathbf{u} - 2\mu i p_x u_x + \sigma M \nabla \mathbf{w}, \\ \tau_{zx} &= \mu(i p_x u_z + u'_x), \\ -p_f &= \sigma M \nabla \mathbf{u} + M \nabla \mathbf{w}. \end{aligned} \quad (10)$$

According to our starting point, $\nabla \mathbf{u} = ip_x u_x + u'_z$ and $\nabla \mathbf{w} = ip_x w_x + w'_z$. Furthermore, we transform the second-order Biot differential equations to a system of first-order differential equations, as is common in the elastic case (see, e.g., Aki and Richards, 1980). The medium is now characterized by

$$\frac{d\zeta}{dz} + \mathbf{P}\zeta = 0. \quad (11)$$

Here, $\zeta = (u_x, u_z, w_z, \tau_{xz}, \tau_{zx}, p_f)^T$ and \mathbf{P} is a (6×6) matrix, consisting of combinations of the above-defined layer parameters and describing the P - and SV -wave propagation. The exact expressions for \mathbf{P} and for the equation that describes SH -waves are given in the Appendix.

TI effective medium

Next, we consider instead of the single layer the whole stack of layers in the long-wavelength (i.e., effective-medium) limit. As we did for each single layer, we can write the Biot equations for a homogeneous, anisotropic medium that will be identified as the effective medium, replacing the layered one after averaging. For isotropic layers and for TIV layers (which are transversely isotropic and have a vertical symmetry axis as the stack of layers), this medium is determined by eight poroelastic constants $B_1^*, B_2^*, \dots, B_8^*$ and two effective directional permeabilities k_z^* and k_{xy}^* . $B_1^*, B_2^*, \dots, B_8^*$ are defined according to Biot (1962), and the TIV stress-strain relations are

$$\begin{aligned} \tau_{xx} &= ip_x(2B_1^* + B_2^*)u_x + B_3^*u'_z - B_6^*\nabla \mathbf{w}, \\ \tau_{yy} &= ip_x B_2^*u_x + B_3^*u'_z - B_6^*\nabla \mathbf{w}, \\ \tau_{zz} &= ip_x B_3^*u_x + B_4^*u'_z - B_7^*\nabla \mathbf{w}, \\ \tau_{zx} &= B_5^*(ip_x u_z + u'_x), \\ -p_f &= ip_x B_6^*u_x + B_7^*u'_z - B_8^*\nabla \mathbf{w}. \end{aligned} \quad (12)$$

With starting point similar to that of equation (8), a matrix \mathbf{P}^* is determined. \mathbf{P}^* characterizes the anisotropic effective medium with respect to the qP - and qSV -wave propagation and is defined in the Appendix together with the SH -wave equation. Since we are interested in solutions in the zero frequency limit, we can use the condition $\zeta^* = \langle \zeta \rangle$. We identify the above-defined TI medium as the effective medium that replaces the heterogeneous medium after averaging, so that

$$\mathbf{P}^* = \langle \mathbf{P} \rangle. \quad (13)$$

ISOTROPIC LAYERS

We compare both matrices element by element by keeping only the terms of lowest order in frequency. In this way, we find the effective poroelastic constants and simple relations for the densities $\rho^* = \langle \rho \rangle$ and $\rho_f^* = \langle \rho_f \rangle$. The results for the permeability in q_{xy}^* and q_z^* are discussed below.

Effective medium: Quasi-static limit

The quasi-static effective poroelastic constants are

$$\begin{aligned} B_1^* &= \langle \mu_d \rangle, \\ B_2^* &= 2 \left\langle \frac{\lambda_d \mu_d}{\lambda_d + 2\mu_d} \right\rangle + \left\langle \frac{\lambda_d}{\lambda_d + 2\mu_d} \right\rangle^2 \left\langle \frac{1}{\lambda_d + 2\mu_d} \right\rangle^{-1} + \frac{B_6^{*2}}{B_8^*}, \\ B_3^* &= \left\langle \frac{\lambda_d}{\lambda_d + 2\mu_d} \right\rangle \left\langle \frac{1}{\lambda_d + 2\mu_d} \right\rangle^{-1} + \frac{B_6^* B_7^*}{B_8^*}, \\ B_4^* &= \left\langle \frac{1}{\lambda_d + 2\mu_d} \right\rangle^{-1} + \frac{B_7^{*2}}{B_8^*}, \\ B_5^* &= \langle \mu_d^{-1} \rangle^{-1}, \\ B_6^* &= -B_8^* \left(2 \left\langle \frac{\sigma \mu_d}{\lambda_d + 2\mu_d} \right\rangle \right. \\ &\quad \left. + \left\langle \frac{\sigma}{\lambda_d + 2\mu_d} \right\rangle \left\langle \frac{\lambda_d}{\lambda_d + 2\mu_d} \right\rangle \left\langle \frac{1}{\lambda_d + 2\mu_d} \right\rangle^{-1} \right), \\ B_7^* &= -B_8^* \left\langle \frac{\sigma}{\lambda_d + 2\mu_d} \right\rangle \left\langle \frac{1}{\lambda_d + 2\mu_d} \right\rangle^{-1}, \\ B_8^* &= \left[\langle M^{-1} \rangle + \left\langle \frac{\sigma^2}{\lambda_d + 2\mu_d} \right\rangle \right. \\ &\quad \left. - \left\langle \frac{\sigma}{\lambda_d + 2\mu_d} \right\rangle^2 \left\langle \frac{1}{\lambda_d + 2\mu_d} \right\rangle^{-1} \right]^{-1}. \end{aligned} \quad (14)$$

B_1^* and B_5^* are the same as Backus' M_B and L_B , respectively, but with shear moduli of the dry poroelastic frame. B_2^* , B_3^* , and B_4^* are poroelastic generalization of Backus's B_B , F_B , and C_B , respectively, but with additional terms (combinations of B_6^* , B_7^* , and B_8^*) that introduce effects of fluid saturation (M) and the difference between matrix and grain compressibilities (σ). For dry rock, $B_6^* = B_7^* = 0$. To check the result with Gassman's formula, one can apply the formalism to a model in which all layers are identical. In this case, the averaging brackets can be omitted and the expected results $B_8^* = M$, $B_7^* = B_6^* = \sigma M$, $B_4^* = H$, $B_2^* = B_3^* = H - 2\mu$, and $B_1^* = B_5^* = \mu$ can be derived easily. Upscaling from log to surface seismic frequencies should be done using the effective moduli of equation (14) if the seismic frequencies are lower than ω_0 .

Effective medium: No-flow limit

For frequencies above ω_0 , the interfaces between different layers behave as isolating with respect to interlayer flow. This means that in equation (10) as well as in the corresponding TIV equations (12), $\nabla \mathbf{w} \equiv 0$ (as proposed by Norris, 1993). The matrices \mathbf{P} and \mathbf{P}^* are defined in the same ways as in the quasi-static limit, but the condition $\nabla \mathbf{w} \equiv 0$ here leads to great simplifications. The medium is characterized by the saturated poroelastic constants of each layer itself, and averaging must be performed over those saturated (Gassmann) moduli. The result corresponds to a "naive" application of the standard Backus formalism, which ignores fluid flow. In certain cases, it can differ significantly from the static one derived above. It is compared with the former in Figures 2 to 8 and discussed below. Because of the no-flow condition $\nabla \mathbf{w} \equiv 0$, the poroelastic constant B_8^* no longer plays any part in the stress-strain relations, and the remaining seven high-frequency moduli are defined as

$$\begin{aligned}
 B_1^* &= \langle \mu_d \rangle, \\
 B_2^* &= 2 \left\langle \frac{(H - 2\mu_d)\mu_d}{H} \right\rangle + \left\langle \frac{H - 2\mu_d}{H} \right\rangle^2 \left\langle \frac{1}{H} \right\rangle^{-1}, \\
 B_3^* &= \left\langle \frac{H - 2\mu_d}{H} \right\rangle \left\langle \frac{1}{H} \right\rangle^{-1}, \\
 B_4^* &= \left\langle \frac{1}{H} \right\rangle^{-1}, \\
 B_5^* &= \langle \mu_d^{-1} \rangle^{-1}, \\
 B_6^* &= B_7^* = \left\langle \frac{1}{\sigma M} \right\rangle^{-1}.
 \end{aligned}
 \tag{15}$$

Elastic Backus averaging, which ignores fluid effects such as interlayer flow, is useful for upscaling from sonic log velocities to VSP or crosshole seismic applications (see, e.g., Pratt and Sams, 1996; Rio et al., 1996; Tang and Burns, 1992). It can be applied if the frequencies are higher than ω_0 . It should be noted here that the results of no-flow averaging [equations (15)] also follow from the poroelastic generalized O'Doherty-Anstey formulas (Gelinsky and Shapiro, 1997) for frequencies $\omega > \omega_0$ without any a priori assumptions regarding $\nabla \mathbf{w}$.

The quasi-static as well as the no-flow moduli are derived consistently by combination of low-frequency Biot- theory and

Backus averaging for $\omega_0 < \omega_c$. If the medium parameters are such that $\omega_0 > \omega_c$, a high-frequency Biot correction must be applied. The result is then a heuristic combination of both methods, and the averaging [equations (15)] has only a formal character.

Geertsma and Smit (1961) derived an approximate correction factor v_∞/v_0 that is written, in our notation, as

$$\frac{v(\omega \rightarrow \infty)}{v(\omega \rightarrow 0)} = \sqrt{\frac{a - 2 \frac{\phi \sigma M}{H} + \frac{\phi M \rho}{H \rho_f}}{a - \frac{\phi \rho_f}{\rho}}}. \tag{16}$$

For well-consolidated rocks with low porosity and high tortuosity, this factor is close to unity. For weak, highly porous materials, however, Biot dispersion can be greater than 10%. The multiplication of v_P by such a correction factor ignores any influence of anisotropy on the global flow dispersion. Gelinsky and Shapiro (1996) showed that at least the anisotropy of permeability (which is stronger than poroelastic anisotropy layered systems; see below) does not affect v_∞/v_0 .

High-frequency limit: Ray theory

To conclude this section, the ray-theory limit is considered briefly. Since the frequency is high, no equilibration of fluid pressure can take place. The layers are isolated as before, in the no-flow limit. The difference from the previously considered no-flow limit is that poroelastic slownesses, not poroelastic moduli, must be averaged. The P -wave phase velocity is defined as $v_{\text{ray}} = (L^2 + X^2)^{1/2}/T$, where L and X are the total vertical and horizontal distances traveled by a ray and T is the total traveltime. According to Shapiro et al. (1994), the velocity can be written as

$$v_{\text{ray}} = c_0 \left(1 + \frac{\sigma_{\alpha\alpha}^2}{2 \cos^2 \theta} \right). \tag{17}$$

Here, $c_0 = (\langle s^2 \rangle)^{-1/2}$ and $\langle s^2 \rangle$ denotes the average over the squared slownesses of each layer. Furthermore, $\sigma_{\alpha\alpha}^2$ is the variance of the layer velocities normalized by the square of the arithmetic average velocity. Equation (17) coincides with the definition for v_{ray} given in the text if higher-than-second-order terms in the fluctuations are neglected. Since v_{ray} is defined in the high-frequency limit ($\omega \rightarrow \infty$), the velocity must be corrected for Biot's global flow dispersion unless the layer slownesses already have been measured in the high-frequency limit.

Liu et al. (1995) discussed the upscaling from ultrasonic to sonic log measurements and compared two modeling schemes—the high-frequency time-average equation (ray theory) and the low-frequency elastic Backus averaging. For this frequency range, they found better agreement of the modeled and the real sonic logs using the short-wavelength scheme.

Weak poroelastic anisotropy

To compare the results of the different averaging schemes, poroelastic velocities are calculated from the moduli derived above. The effective medium can be described by the isotropic,

saturated, poroelastic P - and S -wave velocities α_0 and β_0 , measured parallel to the symmetry axis (i.e., vertically for the TIV medium considered here), and by the Thomsen (1986) anisotropy parameters ϵ , γ , and δ . The velocities α_0 and β_0 can be calculated according to the Gassmann formula (e.g., White, 1983) as

$$\begin{aligned}\alpha_0 &= \sqrt{\frac{B_4^*}{\rho^*}}, \\ \beta_0 &= \sqrt{\frac{B_5^*}{\rho^*}}.\end{aligned}\quad (18)$$

In terms of the poroelastic constants B_i^* , the definitions of poroelastic Thomsen parameters ϵ , γ , and δ are

$$\begin{aligned}\epsilon &= \frac{B_2^* + 2B_1^* - B_4^*}{2B_4^*}, \\ \gamma &= \frac{B_1^* - B_5^*}{2B_5^*}, \\ \delta &= \frac{(B_3^* + B_5^*)^2 - (B_4^* - B_5^*)^2}{2B_4^*(B_4^* - B_5^*)}.\end{aligned}\quad (19)$$

B_1^*, \dots, B_5^* were calculated in the previous sections for anisotropy caused by thin layering. However, the anisotropy parameters defined in equation (19) are valid for any kind of TIV poroelastic media, with B_1^*, \dots, B_5^* being calculated, e.g., according to the method in Brown and Korringa (1975). With these constants, the poroelastic velocities for weak anisotropy can be written simply as

$$\begin{aligned}v_{qP} &= \sqrt{B_4^*/\rho^*} (1 + \delta \sin^2 \theta \cos^2 \theta + \epsilon \sin^4 \theta), \\ v_{qSV} &= \sqrt{B_5^*/\rho^*} \left(1 + \frac{B_4^*}{B_5^*} (\epsilon - \delta) \sin^2 \theta \cos^2 \theta \right), \\ v_{SH} &= \sqrt{B_5^*/\rho^*} (1 + \gamma \sin^2 \theta).\end{aligned}\quad (20)$$

The qSV -wave is not a pure shear wave and hence is affected by fluid saturation by means of B_4^* , ϵ , δ , and ρ^* . The SH -wave as a pure shear mode is affected by fluid effects only through ρ^* , since γ is the same for dry and saturated media. Since in several cases considered here the anisotropy is strong ($\epsilon, \gamma, \delta \gg 10\%$), we used for the figures the exact formula for the qP -wave phase velocity given in Thomsen (1986).

ISOTROPIC LAYERS: DISCUSSION OF RESULTS

For different media, we compared the anisotropic P -wave phase velocities derived from ray theory and from the quasi-static and the no-flow moduli. The rock properties are shown in Table 1, and those of the saturating fluid and gas phases are shown in Table 2. Partial saturation was stimulated by assuming the existence of gas-saturated layers between water-saturated layers (White, 1983). This model seems to be justified, since the bulk modulus of a gas-fluid mixture is rather close to that of the pure gas phase,

$$K_f = \frac{K_{\text{liquid}} K_{\text{gas}}}{S K_{\text{gas}} + (1 - S) K_{\text{liquid}}}, \quad (21)$$

with S being the relative fluid saturation. The velocities are plotted as a function of the angle of incidence θ . The Biot-corrected ray-theory velocity is referred to as ray-Biot, the no-flow limit is referred to as high or high-Biot if $\omega_0 > \omega_c$, and the quasi-static limit is referred to as low. In Figures 2 through 8, v_{ray} is plotted mostly only for $\theta = 0^\circ$ to 60° , since for larger angles of incidence $1/\cos^2 \theta$ becomes huge.

The medium considered in Figure 2 is a homogeneous Berea sandstone, saturated by alternating gas and fluid phases. Layering is caused only by the alternating saturation, and the dry poroelastic properties of all layers are the same. Since the shear strength is constant throughout the medium, both the quasi-static (low) and the no-flow (high) Backus velocities are isotropic. Only the ray-theory limit shows some very weak anisotropy. The no-flow velocity is very close to that predicted by ray theory, whereas the quasi-static velocity is much

Table 2. Fluid and gas properties.

Parameter	Unit	Water ⁽¹⁾	Gas ⁽¹⁾
K_f	10^9 Pa	2.25	0.056
ρ_f	kg/m^3	1000	140
η	$10^{-3} \text{Pa} \times \text{s}$	1.0	0.22

⁽¹⁾Gurevich and Lopatnikov, 1995.

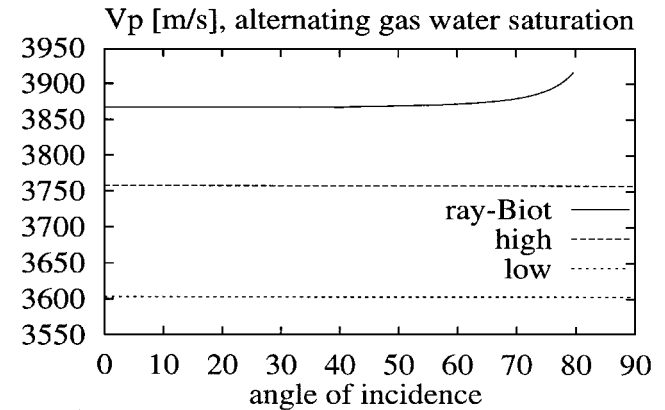


FIG. 2. P -wave velocities for layers of rock type 1 with alternating fluid and gas saturation. In this figure and Figures 3 through 8, low, high, and ray-Biot refer to the respective frequency ranges defined in the text. Rock and fluid properties are listed in Tables 1 and 2.

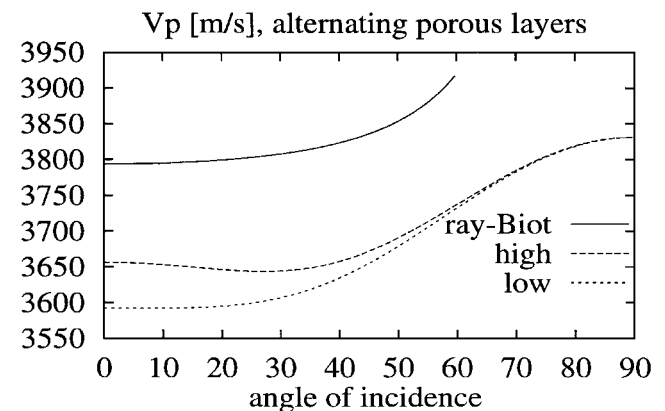


FIG. 3. P -wave phase velocities for alternating layers of different sandstones (rock types 2 and 3), both water saturated.

smaller. Since in this limit interlayer flow from the water- into the gas-saturated layers equilibrates the fluid pressure, no additional stiffness is caused by water saturation, as for the higher frequencies.

The model in Figure 3 is a porous rock made of two types of alternating porous layers. Both layer types are uniformly water saturated. Since there is a significant difference in

shear strength between the layers, the Backus velocities are anisotropic. The exact coincidence of the quasi-static and the no-flow velocities for $\theta = 90^\circ$ is caused by the choice of parameters and is not necessarily the case for other parameters (cf. Figure 6). In this model, the Thomsen parameters are $\epsilon_{low} = 0.069$, $\gamma_{low} = 0.092$, $\delta_{low} = -0.002$, $\epsilon_{high} = 0.049$, $\gamma_{high} = \gamma_{low}$, and $\delta_{high} = -0.033$.

0 In Figure 4, the same rock model as that in Figure 3 is considered, but here the stiffer layers are assumed to be water saturated and the weaker (more compliant) layers are assumed to be gas saturated. The anisotropy of the ray-theory and no-flow velocities is slightly increased because of the increased contrast of the different layer properties. In the quasi-static limit, interlayer flow tends to reduce the enhanced elastic contrast, and the anisotropy is reduced compared with that at higher frequencies. All velocities are smaller than in the fully water-saturated example. The Thomsen parameters are (with γ as in Figure 3) $\epsilon_{low} = 0.11$, $\delta_{low} = 0.014$, $\epsilon_{high} = 0.14$, and $\delta_{high} = 0.038$.

In Figure 5, the saturation pattern of Figure 4 is reversed. Here the stiffer layers are assumed to be gas saturated, and the weaker layers are assumed to be water saturated. As a result, the contrast between isolated layers is significantly smaller than in Figure 4 and Figure 3. Both the ray-theory and the no-flow velocities are less anisotropic. Because of the equilibrating interlayer flow, however, the quasistatic velocity and the

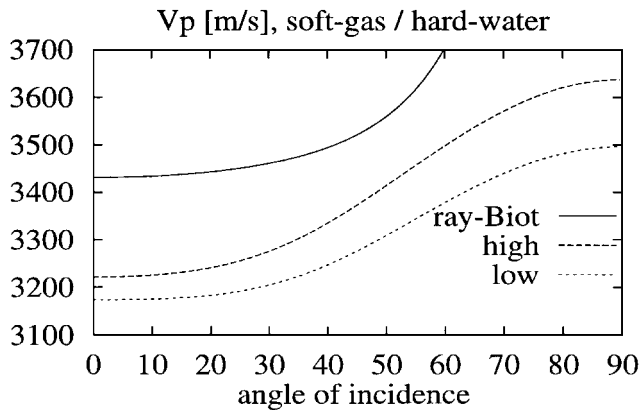


FIG. 4. Same as Figure 3, but with water-saturated layers of type 2 (stiff) and gas-saturated layers of type 3 (weak).

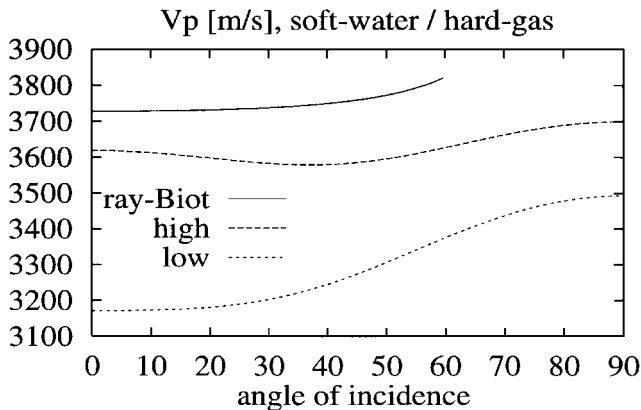


FIG. 5. Same as Figure 3, but with gas-saturated layers of type 2 (stiff) and water-saturated layers of type 3 (weak).

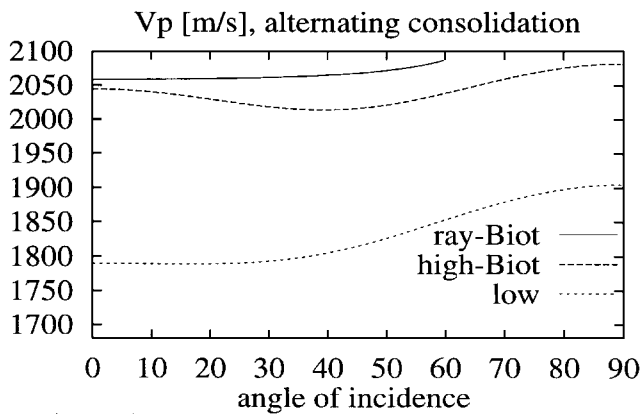


FIG. 6. *P*-wave phase velocities for alternating layers consisting of weak sandstone and of unconsolidated coarse sand (rock types 4 and 5), both water saturated. Both the no-flow and the ray-theory limits are corrected for Biot dispersion.

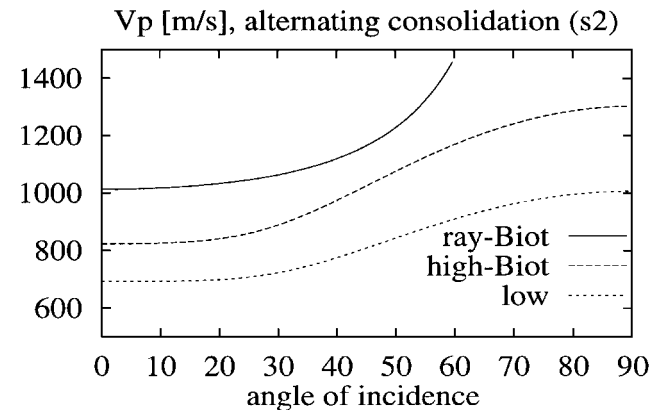


FIG. 7. Same as Figure 6, but with water-saturated layers of type 4 (stiff) and gas-saturated layers of type 5 (weak).

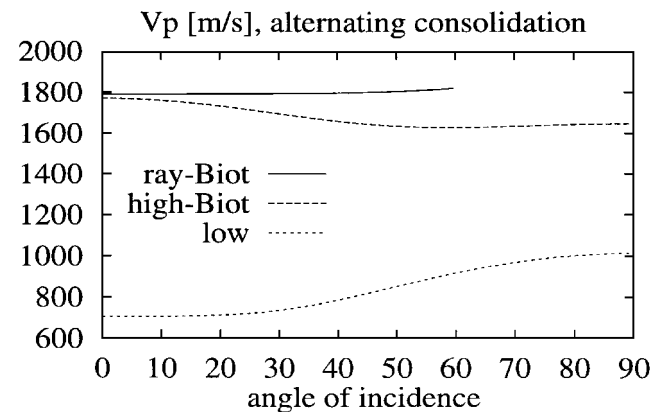


FIG. 8. Same as Figure 6, but with gas-saturated layers of type 4 (stiff) and water-saturated layers of type 5 (weak).

low-frequency Thomsen parameters are the same as in Figure 4. For the high frequencies, the parameters are $\epsilon_{\text{high}} = 0.023$ and $\delta_{\text{high}} = -0.056$; γ is again the same.

These effects can be studied for many other models. For example, Figure 6 describes alternating sand layers with different degrees of consolidation and shear strength. In this model, $\omega_0 > \omega_c$, so the no-flow limit is corrected for the (quite significant) global flow dispersion. As noted above, in this case the no-flow limit has only a formal character. We provide the corresponding curves in order to show the contrast with the quasi-static limit. In Figures 7 and 8, the effects of partial saturation are investigated for this model and are found to be similar to those shown in Figures 4 and 5. The unusual angle dependence of v_p here is caused by the very small shear moduli. We have investigated more models and basically found the same effects as in the chosen examples. Our results are in agreement with the six rigorous constraints on elastic stiffnesses that must be fulfilled for any stable TIV medium (Berge, 1995; Helbig, 1994).

For vertical incidence, the velocity dispersion and attenuation of compressional waves in partially saturated media can be calculated as a function of frequency (Dutta and Odé, 1979; Gurevich and Lopatnikov, 1995; Gelinsky and Shapiro, 1997). The results presented here are special cases of these theories with respect to frequency dependence (only limits such as the quasi-static velocity for $\omega \rightarrow 0$ can be obtained). However, anisotropy and nonvertical incidence also are covered. For example, the quasi-static and the no-flow velocities for $\theta = 0^\circ$ in Figures 2 and 3 coincide with the corresponding limits derived by Gurevich and Lopatnikov (1995), who considered the same model only for vertical incidence.

ANISOTROPIC LAYERS

TIV layers (TI layers with a vertical symmetry axis)

We first consider layers that are TIV themselves. For elastic layers, the same problem was treated explicitly in Backus (1962), and Helbig (1994) provided a recipe for elastic Backus averaging for any kind of layer anisotropy. Typical media with TIV layers may be sediments containing shale, which is itself anisotropic (Hornby et al., 1994; Schoenberg et al., 1996). The combined effect of intrinsic anisotropy and layering also has been observed in VSP data (Kebaili and Schmitt, 1996) and in crosshole data (Pratt and Sams, 1996). To parameterize each layer, the five constants b_d , c_d , f_d , ℓ_d , and m_d are necessary. These are the corresponding Backus constants of the dry rock matrix. In the standard elastic notation they are $b \doteq C_{11}$, $c \doteq C_{33}$, $f \doteq C_{13}$, $l \doteq C_{44}$, and $m \doteq C_{66}$. Furthermore, for each layer, P , Q , and R are introduced (they are analogous to B_6^* , B_7^* , and B_8^* for the TI effective medium described in the previous section). Carcione (1995) described how to determine the constants P , Q , and R (in his notation, $\alpha_1 M$, $\alpha_3 M$, and M) as a function of the anisotropic dry matrix moduli. The properties of the effective medium are calculated in the same way as for isotropic layers. The TIV poroelastic quasi-static effective-medium constants are

$$B_1^* = \langle m_d \rangle,$$

$$B_2^* = \langle b_d - f_d^2 c_d^{-1} \rangle + \langle f_d c_d^{-1} \rangle^2 \langle c_d^{-1} \rangle^{-1} + \frac{B_6^{*2}}{B_8^*},$$

$$B_3^* = \langle f_d c_d^{-1} \rangle \langle c_d^{-1} \rangle^{-1} + \frac{B_6^* B_7^*}{B_8^*},$$

$$B_4^* = \langle c_d^{-1} \rangle^{-1} + \frac{B_7^{*2}}{B_8^*},$$

$$B_5^* = \langle \ell_d^{-1} \rangle^{-1},$$

$$B_6^* = B_8^* \left(\left\langle \frac{P}{R} \right\rangle - \left\langle \frac{Q}{R} f_d c_d^{-1} \right\rangle + \left\langle \frac{Q}{R} c_d^{-1} \right\rangle \langle f_d c_d^{-1} \rangle \langle c_d^{-1} \rangle^{-1} \right),$$

$$B_7^* = B_8^* \left\langle \frac{Q}{R} c_d^{-1} \right\rangle \langle c_d^{-1} \rangle^{-1},$$

$$B_8^* = \left[\langle R^{-1} \rangle + \left\langle \frac{Q^2}{R^2} c_d^{-1} \right\rangle - \left\langle \frac{Q}{R} c_d^{-1} \right\rangle^2 \langle c_d^{-1} \rangle^{-1} \right]^{-1}.$$

As for isotropic layers, limiting no-flow modulus and ray-theory velocities can be calculated. Starting points for the derivation of no-flow moduli are the anisotropic saturated Gassmann moduli given by Brown and Korrington (1975).

TIH (TI with a horizontal symmetry axis) layers with fractures

Finally, we generalize our approach for layers that are poroelastic and fractured with the horizontal x -axis as the symmetry axis of the fracturing (TIH layers). The fractures are perpendicular to the symmetry axis of the layering itself (cf. Figure 1). The resulting effective medium is orthorhombic, determined by 13 poroelastic constants (making use of the fact that the anisotropy is caused by fracturing reduces the number of independent constants to 12) and three values for the directional permeability. The aligned fractures are assumed to cause only anisotropy of the poroelastic frame and of the permeability (flow channel). No distinction between a soft fracture porosity and the stiffer background porosity is made here.

We parameterize the TIH layers according to Biot (1962) by using B_1 , B_2 , ..., B_8 , keeping in mind that now the x -axis instead of the z -axis is the symmetry axis for the layers. B_1 , B_2 , ..., B_5 can be determined by adding the tangential and normal excess compliances caused by fracturing to an isotropic background compliance (Schoenberg and Sayers, 1995). Following Thomsen (1995), the anisotropic poroelastic constants of a saturated medium with aligned fractures can be expressed in terms of the parameters ϵ , γ , and δ . The remaining three constants B_6 , B_7 , and B_8 can be measured (Biot and Willis, 1957) or calculated using micromechanical models (see, e.g., Yew and Weng, 1987).

The effective medium is orthorhombic and described by nine poroelastic constants A_{ij}^* and the four Biot constants M_i^* (notation according to Biot, 1962). Since displacements in the y -direction are not equivalent to those in the x -direction, in equation (8) for \mathbf{u} and \mathbf{w} , u_y , w_y , and p_y are retained. After transformation to first-order differential equations, the vector ζ is defined as

$$\zeta = (u_x, u_y, u_z, w_z, \tau_{xz}, \tau_{yz}, \tau_{zz}, p_f)^T, \quad (23)$$

and \mathbf{P} and \mathbf{P}^* are (8×8) matrices consisting of combinations of the above-defined layer parameters, as in the previous case. Here we denote the dry-layer stiffnesses with a tilde on top [see equation (A-2) of the Appendix for definitions of \tilde{B}_2 , \tilde{B}_3 , and \tilde{B}_4]. Furthermore, $\tilde{B}_b = \tilde{B}_2 + 2\tilde{B}_1$. After comparing all

elements of $\langle \mathbf{P} \rangle$ and \mathbf{P}^* and solving the corresponding equations for A_{ij}^* and M_i^* , the orthorhombic quasi-static effective medium is defined by

$$\begin{aligned}
 A_{11}^* &= \langle \tilde{B}_4 \rangle + \left\langle \frac{\tilde{B}_3}{\tilde{B}_b} \right\rangle^2 \langle \tilde{B}_b^{-1} \rangle^{-1} - \left\langle \frac{\tilde{B}_3^2}{\tilde{B}_b} \right\rangle + \frac{M_1^{*2}}{M^*}, \\
 A_{22}^* &= \langle \tilde{B}_b \rangle + \left\langle \frac{\tilde{B}_2}{\tilde{B}_b} \right\rangle^2 \langle \tilde{B}_b^{-1} \rangle^{-1} - \left\langle \frac{\tilde{B}_2^2}{\tilde{B}_b} \right\rangle + \frac{M_2^{*2}}{M^*}, \\
 A_{33}^* &= \langle \tilde{B}_b^{-1} \rangle^{-1} + \frac{M_3^{*2}}{M^*}, \\
 A_{12}^* &= \langle \tilde{B}_3 \rangle + \left\langle \frac{\tilde{B}_3}{\tilde{B}_b} \right\rangle \left\langle \frac{\tilde{B}_2}{\tilde{B}_b} \right\rangle \langle \tilde{B}_b^{-1} \rangle^{-1} - \left\langle \frac{\tilde{B}_3 \tilde{B}_2}{\tilde{B}_b} \right\rangle + \frac{M_1^* M_2^*}{M^*}, \\
 A_{13}^* &= \left\langle \frac{\tilde{B}_3}{\tilde{B}_b} \right\rangle \langle \tilde{B}_b^{-1} \rangle^{-1} + \frac{M_1^* M_3^*}{M^*}, \\
 A_{23}^* &= \left\langle \frac{\tilde{B}_2}{\tilde{B}_b} \right\rangle \langle \tilde{B}_b^{-1} \rangle^{-1} + \frac{M_2^* M_3^*}{M^*}, \\
 A_{44}^* &= \left\langle \frac{1}{\tilde{B}_1} \right\rangle^{-1}, \\
 A_{55}^* &= \left\langle \frac{1}{\tilde{B}_5} \right\rangle^{-1}, \\
 A_{66}^* &= \langle \tilde{B}_5 \rangle, \\
 M_1^* &= M^* \left(\left\langle \frac{B_7}{B_8} \right\rangle - \left\langle \frac{B_6 \tilde{B}_3}{B_8 \tilde{B}_b} \right\rangle + \left\langle \frac{B_6}{B_8 \tilde{B}_b} \right\rangle \left\langle \frac{\tilde{B}_3}{\tilde{B}_b} \right\rangle \langle \tilde{B}_b^{-1} \rangle^{-1} \right), \\
 M_2^* &= M^* \left(\left\langle \frac{B_6}{B_8} \right\rangle - \left\langle \frac{B_6 \tilde{B}_2}{B_8 \tilde{B}_b} \right\rangle + \left\langle \frac{B_6}{B_8 \tilde{B}_b} \right\rangle \left\langle \frac{\tilde{B}_2}{\tilde{B}_b} \right\rangle \langle \tilde{B}_b^{-1} \rangle^{-1} \right), \\
 M_3^* &= M^* \left(\left\langle \frac{B_6}{B_8 \tilde{B}_b} \right\rangle \langle \tilde{B}_b^{-1} \rangle^{-1} \right), \\
 M^* &= \left[\left\langle \frac{1}{B_8} \right\rangle + \left\langle \frac{B_6^2}{B_8^2 \tilde{B}_b} \right\rangle - \left\langle \frac{B_6}{B_8 \tilde{B}_b} \right\rangle^2 \langle \tilde{B}_b^{-1} \rangle^{-1} \right]^{-1}.
 \end{aligned} \tag{24}$$

The corresponding moduli for higher frequencies can be calculated as described above for TIV layers (keeping in mind the different symmetry properties).

ANISOTROPIC PERMEABILITY

The formalism that was introduced above yields (in addition to the poroelastic constants of the long-wavelength effective medium) simple relations for an anisotropic permeability. These are valid in the quasi-static limit and are useful for the description of fluid flow resulting from a constant or slowly varying pressure gradient. For higher frequencies, the

propagation of seismic waves is influenced by a dynamic permeability (Johnston et al., 1987; Smeulders et al., 1992).

We first consider isotropic layers. The relation $\langle \mathbf{P} \rangle = \mathbf{P}^*$ yields, besides the poroelastic constants for the effective, anisotropic Darcy coefficient (the ratio of permeability to viscosity),

$$\begin{aligned}
 \left(\frac{k_{xy}}{\eta} \right)^* &= \left\langle \frac{k}{\eta} \right\rangle, \\
 \left(\frac{k_z}{\eta} \right)^* &= \left\langle \left(\frac{k}{\eta} \right)^{-1} \right\rangle^{-1}.
 \end{aligned} \tag{25}$$

Thus, the inverse of the permeability behaves just like electrical resistors connected either in series or in parallel. For constant fluid viscosity throughout the medium, η can be canceled on both sides of equation (25) and the results of Schoenberg (1991) for layered permeable systems, derived from Darcy's law, are reproduced. If the viscosity of the saturating fluid varies from layer to layer, it will affect the effective Darcy coefficient and should be considered. As an example, we study fluctuations of porosity from layer to layer and keep the other fluid parameters, such as bulk modulus, viscosity, and density, constant throughout the medium. If the permeability depends in a simple way on porosity, k_{xy}^* and k_z^* can be derived as functions of porosity fluctuations. We assume a permeability-porosity dependence of a Kozeny-Carman type (Scheidegger, 1974), in that

$$k_0 = \frac{1}{C^2} \frac{\phi_0^3}{(1 - \phi_0)^2}. \tag{26}$$

Here, ϕ_0 is a constant porosity (as the average or background porosity of the layered system) and the constant C (termed flow-zone indicator) is inversely proportional to the product of tortuosity, the ratio of pore surface area to grain volume, and the square root of a capillary shape factor (Georgi and Menger, 1994). We study porosity fluctuations $\phi_0(1 + \Delta_\phi(z))$ with fluctuations for which the average over z equals zero, $\langle \Delta_\phi \rangle = 0$. Additionally, we assume $\langle \Delta_\phi^2 \rangle \ll 1$ and neglect higher-order statistical moments. Assuming also a constant flow-zone indicator C throughout the medium, the directional permeability is

$$k_{xy}^* = k_0 \left(1 + \langle \Delta_\phi^2 \rangle \frac{3}{(1 - \phi_0)^2} \right), \tag{27}$$

$$k_z^* = k_0 \left(1 + \langle \Delta_\phi^2 \rangle \frac{6 - 6\phi_0 + \phi_0^2}{(1 - \phi_0)^2} \right)^{-1}. \tag{28}$$

In Figure 9, the ratio k_{xy}^*/k_z^* is plotted as a function of porosity fluctuations $(\Delta_\phi^2)^{1/2}$. The average porosity varies as $\phi_0 = 0.4, 0.3, 0.2,$ and 0.1 . The ratio k_{xy}^*/k_z^* defines the anisotropic permeability and is independent of k_0 . Both k_{xy}^* (upper curves) and k_z^* (lower curves), normalized by k_0 , are plotted in Figure 10. From above and below toward the center, the average porosity decreases, as in Figure 9, from 0.4 to 0.1. Whereas k_{xy}^*/k_0 is increasing with increasing fluctuations, k_z^*/k_0 is decreasing. Whereas k_{xy}^*/k_0 is strongly increasing with a growing average porosity, k_z^*/k_0 is approximately independent of ϕ_0 , although $k_0 \rightarrow 0$ with ϕ_0 . An anisotropic permeability may significantly affect the propagation of seismic waves (Hamdi and Taylor

Smith, 1982; Gibson and Toksöz, 1990; Gelinsky and Shapiro, 1996; Carcione, 1995).

For the fractured medium, the permeability of each layer already is anisotropic. The (larger) permeability parallel to the fracture planes is k_{yz} , whereas k_x is the (smaller) one perpendicular to the fractures. The elements of the permeability tensor of an orthorhombic effective medium in the case of constant viscosity are

$$\begin{aligned} k_x^* &= \langle k_x \rangle, \\ k_y^* &= \langle k_{yz} \rangle, \\ k_z^* &= \langle k_{yz}^{-1} \rangle^{-1}. \end{aligned} \quad (29)$$

Layers that possess TIV poroelastic parameters, for instance, because of their high shale content, can be approximated by isotropic layers with respect to permeability. Alternating sand and shale layers with alternating very high and very low

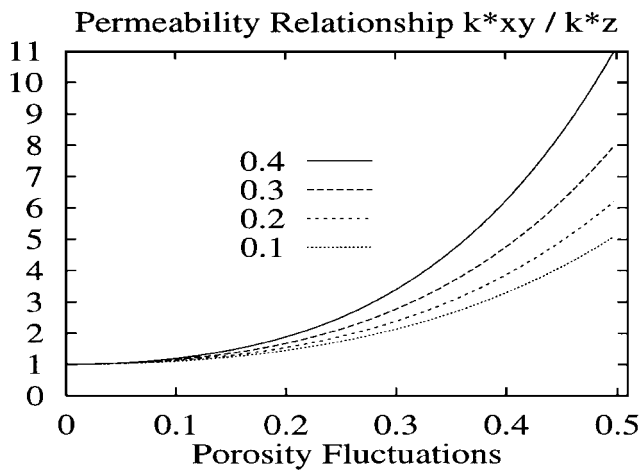


FIG. 9. Ratio of the permeabilities parallel and perpendicular to the layering as a function of porosity fluctuations. Average porosity decreases from 0.4 to 0.1 (top to bottom).

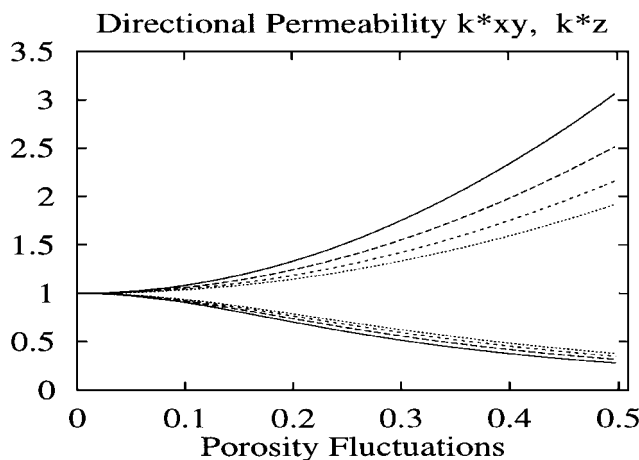


FIG. 10. Directional permeabilities (k_{xy}^* parallel and k_z^* perpendicular to the layering) normalized by k_0 for a stack of isotropic layers as a function of porosity fluctuations [equations (27) and (28) with ϕ_0 as in Figure 9].

permeabilities may cause an effectively strong anisotropic permeability.

CONCLUSION

Simple expressions for the effective poroelastic constants of thinly layered and poroelastic, fluid-saturated media were derived. Application of Backus averaging implies the assumption that the seismic wavelength is much greater than the characteristic length of medium heterogeneities. This scale can be given by the layer thickness, period, or correlation length. Because of fluid flow, especially in partially saturated media, another characteristic length (correspondingly, a frequency) that governs the so-called interlayer flow is involved. Depending on whether the frequency is below or above this characteristic frequency ω_0 , the medium is found to behave differently. This effect is of first-order significance and is observable in the seismic frequency range. Especially in partially saturated media, it may strongly affect the absolute values of seismic velocities as well as their anisotropy. Above ω_0 , no fluid flow occurs and Backus averaging replaces the elastic with the saturated poroelastic constants. Below ω_0 , the diffusive Biot slow wave equilibrates the fluid pressure and quasi-static Backus averaging should be done in the context of Biot theory as outlined in this paper. Fluctuations of porosity are found to be an indication of permeability anisotropy. This anisotropy is much stronger than the corresponding poroelastic anisotropy.

ACKNOWLEDGMENTS

We acknowledge the financial support of STATOIL (Norway) and the German BMBF in the framework of the German-Norwegian Project, Phase II.

REFERENCES

- Aki, K., and Richards, P. G., 1980, Quantitative seismology: W. H. Freeman & Co.
- Backus, G. E., 1962, Long-wave elastic anisotropy produced by horizontal layering: *J. Geophys. Res.*, **67**, 4427-4441.
- Berge, P. A., 1995, Constraints on elastic parameters and implications for lithology in VTI media: 65th Ann. Internat. Mtg., Soc. Expl. Geophys., Expanded Abstracts, 906-909.
- Biot, M., 1956a, Theory of propagation of elastic waves in a fluid-saturated porous solid, I. Low-frequency range: *J. Acoust. Soc. Am.*, **28**, 168-178.
- 1956b, Theory of propagation of elastic waves in a fluid-saturated porous solid, II. Higher-frequency range: *J. Acoust. Soc. Am.*, **28**, 179-191.
- 1962, Mechanics of deformation and acoustic propagation in porous media: *J. Appl. Phys.*, **33**, 1482-1498.
- Biot, M., and Willis, D., 1957, The elastic coefficients of the theory of consolidation: *J. Appl. Mech.*, **24**, 594-601.
- Bourbié, T., Coussy, O., and Zinzner, B., 1987, Acoustics of porous media: Ed. Technip.
- Brown, R., and Korrington, J., 1975, On the dependence of the elastic properties of a porous rock on the compressibility of the pore fluid: *Geophysics*, **40**, 608-616.
- Bruggemann, D. A. G., 1937, Berechnung verschiedener physikalischer Konstanten von heterogenen Substanzen. Teil 3: Die elastischen Konstanten der quasi-isotropen Mischkörper: *Ann. Phys.*, **5**, 160-169.
- Carcione, J. M., 1995, Wave simulation in anisotropic, saturated, porous media: 65th Ann. Internat. Mtg., Soc. Expl. Geophys., Expanded Abstracts, 1309-1312.
- Chandler, R., and Johnson, D. L., 1981, The equivalence of quasi-static flow in fluid saturated porous media and Biot's slow wave in the limit of zero frequency: *J. Appl. Phys.*, **52**, 3391-3395.

- Dewan, J., 1983, Essentials of modern open-hole log interpretation: PennWell Publ. Co.
- Dutta, N. C., and H. Odé, 1979, Attenuation and dispersion of compressional waves in fluid-filled rocks with partial gas saturation (White model)—Parts I and II: *Geophysics*, **44**, 1777–1805.
- Frenkel, J., 1944, On the theory of seismic and seismoelectric phenomena in a moist soil: *J. Phys. (Moscow)*, **8**, 230–241.
- Geertsma, J., and Smit, D., 1961, Some aspects of elastic wave propagation in fluid-saturated porous solids: *Geophysics*, **26**, 169–181.
- Gelinsky, S., and Shapiro, S. A., 1996, Anisotropic permeability: Influence on seismic velocity and attenuation: *Soc. Expl. Geophys., SEG Special Volume on Seismic Anisotropy*, 433–461.
- Gelinsky, S., and Shapiro, S. A., 1997, Dynamic equivalent medium approach for thinly layered saturated sediments: *Geophys. J. Internat.*, **128**, F1–F4.
- Georgi, D., and Menger, S., 1994, Reservoir quality, porosity and permeability relationships, *in* Dresen, L., Fertig, J., Rüter, H., and Budach, W., Eds., 14th Mintrop Seminar, Interpretationsstrategien in Exploration und Produktion.
- Gibson, R., and Toksöz, M., 1990, Permeability estimation from velocity anisotropy in fractured rock: *J. Geophys. Res.*, **95**, 15 643–15 655.
- Gurevich, B., and Lopatnikov, S. L., 1995, Velocity and attenuation of elastic waves in finely layered porous rocks: *Geophys. J. Internat.*, **121**, 933–947.
- Hamdi, F., and Taylor Smith, D., 1982, The influence of permeability on compressional wave velocity in marine sediments: *Geophys. Prosp.*, **30**, 622–640.
- Helbig, K., 1994, Foundations of anisotropy for exploration seismics. Handbook of geophysical exploration. Pergamon Press, Inc.
- Hornby, B. E., Schwartz, L. M., and Hudson, J. A., 1994, Anisotropic effective-medium modeling of elastic properties of shales: *Geophysics*, **59**, 1570–1583.
- Johnston, D. L., Koplik, J., and Daschen, R., 1987, Theory of dynamic permeability and tortuosity in fluid saturated porous media: *J. Fluid Mech.*, **176**, 379–400.
- Kebaili, A., and Schmitt, D. R., 1996, Velocity anisotropy observed in wellbore seismic arrivals: Combined effects of intrinsic properties and layering: *Geophysics*, **61**, 12–20.
- Liu, X., Vernik, L., and Nur, A., 1995, Petrophysical properties of the Monterey formation and fracture detection from the sonic log: 65th Ann. Internat. Mtg., Soc. Expl. Geophys., Expanded Abstracts, 227–230.
- Marion, D., Mukerji, T., and Mavko, G., 1994, Scale effects on velocity dispersion: From ray to effective-medium theories in stratified media: *Geophysics*, **59**, 1613–1619.
- Mukerji, T., and Mavko, G., 1994, Pore fluid effects on seismic velocity in anisotropic rocks: *Geophysics*, **59**, 233–244.
- Norris, A. N., 1993, Low-frequency dispersion and attenuation in partially saturated rocks: *J. Acoust. Soc. Am.*, **94**, 359–370.
- Pratt, R. G., and Sams, M. S., 1996, Reconciliation of crosshole seismic velocities with well information in a layered sedimentary environment: *Geophysics*, **61**, 549–560.
- Rasolofosaon, P., 1991, Plane acoustic waves in linear viscoelastic porous media: Energy, particle displacement, and physical interpretation: *J. Acoust. Soc. Am.*, **89**, 1532–1550.
- Rio, P., Mukerji, T., Mavko, G., and Marion, D., 1996, Velocity dispersion and upscaling in a laboratory-simulated VSP: *Geophysics*, **61**, 584–593.
- Sams, M. S., 1995, Attenuation and anisotropy: The effect of extra-fine layering: *Geophysics*, **60**, 1646–1655.
- Scheidegger, A. E., 1974, The physics of flow through porous media: Univ. of Toronto Press.
- Schoenberg, M., 1991, Layered permeable systems: *Geophys. Prosp.*, **39**, 219–240.
- Schoenberg, M., and Douma, J., 1988, Elastic wave propagation in media with parallel fractures and aligned cracks: *Geophys. Prosp.*, **36**, 571–590.
- Schoenberg, M., Muir, F., and Sayers, C., 1996, Introducing ANNIE: A simple three-parameter anisotropic velocity model for shales: *J. Seis. Expl.*, **5**, 35–49.
- Schoenberg, M., and Sayers, C., 1995, Seismic anisotropy of fractured rock: *Geophysics*, **60**, 204–211.
- Shapiro, S. A., and Hubral, P., 1996, Elastic waves in thinly layered sediments: The equivalent medium and generalized O'Doherty-Anstey formulas: *Geophysics*, **61**, 1282–1300.
- Shapiro, S. A., Hubral, P., and Zien, H., 1994, Frequency-dependent anisotropy of scalar waves in multilayered media: *J. Seis. Expl.*, **3**, 37–52.
- Smeulders, D. M., Eggels, R. L., and van Dongen, M. E., 1992, Dynamic permeability: Reformulation of theory and new experimental and numerical data: *J. Fluid Mech.*, **245**, 211–227.
- Tang, X., and Burns, D. R., 1992, Seismic scattering and velocity dispersion due to heterogeneous lithology: 62nd Ann. Internat. Mtg., Soc. Expl. Geophys., Expanded Abstracts, 824–827.
- Thomsen, L., 1986, Weak elastic anisotropy: *Geophysics*, **51**, 1954–1966.
- Thomsen, L., 1995, Elastic anisotropy due to aligned cracks in porous rocks: *Geophys. Prosp.*, **43**, 805–829.
- Turgut, A., and Yamamoto, T., 1990, Measurements of acoustic wave velocities and attenuation in marine sediments: *J. Acoust. Soc. Am.*, **87**, 2376–2383.
- Wang, Z., and Nur, A., 1992, Elastic wave velocities in porous media, in *Seismic and acoustic velocities in reservoir rocks, Vol. 2: Theoretical and model studies*: Soc. Expl. Geophys., Geophysics Reprint Series No. 10, 1–35.
- White, J., 1983, *Underground sound, application of seismic waves*: Elsevier Science Publ. Co., Inc.
- Widmaier, M., Müller, T., Shapiro, S. A., and Hubral, P., 1995, Amplitude-preserving migration and elastic P -wave AVO corrected for thin layering: *J. Seis. Expl.*, **4**, 169–177.
- Widmaier, M., Shapiro, S. A., and Hubral, P., 1996, AVO correction for scalar waves in the case of a thinly layered reflector overburden: *Geophysics*, **61**, 520–528.
- Yew, C. H., and Weng, X., 1987, A study of reflection and refraction of waves at the interface of water and porous sea ice: *J. Acoust. Soc. Am.*, **82**, 342–353.

APPENDIX

MATRICES \mathbf{P} AND \mathbf{P}^*

Here we describe in more detail how to calculate the quasi-static properties of the TIV effective medium as a function of isotropic layer parameters. Since for this symmetry the SH -wave propagation is independent from that of the qP and qSV waves, it can be treated separately. All information about the qP - and qSV -waves problem is contained in the matrices \mathbf{P} and \mathbf{P}^* . We simplified our treatment of the problem considerably by confining the wave propagation to the x - z plane (which means setting $p_y, u_y, w_y = 0$). By examination of this “reduced” P - and SV -wave problem, however, the poroelastic parameters B_2^* and B_1^* cannot be determined independently. To find all poroelastic constants, we must study, in addition to the P - and SV -wave problem, SH -waves that propagate along the z -axis with particle dis-

placement in the x -direction. This makes it necessary to define τ_{yy} , which is not an element of ζ , as a function of elements of ζ both for the layers and for the TIV effective medium. These two equations are given at the end of the Appendix.

For problems with a lower symmetry, all wave types are coupled and described by (8×8) matrices \mathbf{P} and \mathbf{P}^* . There is one matrix \mathbf{P} for each layer; however, only the average over all layers, $\langle \mathbf{P} \rangle$, is used to determine the effective-medium properties. Since there exists only one realization of the stack of layers, averaging does not mean ensemble averaging but makes use of the self-averaging properties of seismic wavefield parameters as the phase increment (Gelinsky and Shapiro, 1997). Matrix \mathbf{P} is given for isotropic layers as

$$\underline{\mathbf{P}} = \begin{pmatrix} 0 & -ip_x & \frac{1}{\mu_d} & 0 & 0 & 0 \\ -ip_x \frac{\lambda_d}{\lambda_d + 2\mu_d} & 0 & 0 & \frac{1}{\lambda_d + 2\mu_d} & 0 & \frac{\sigma^2}{\lambda_d + 2\mu_d} \\ -\omega^2 \left(\rho - \frac{\rho_f^2}{q} \right) + 4p_x^2 \frac{\mu_d(\lambda_d + \mu_d)}{\lambda_d + 2\mu_d} & 0 & 0 & -ip_x \frac{\lambda_d}{\lambda_d + 2\mu_d} & 0 & -ip_x \frac{\rho_f}{q} + 2ip_x \frac{\sigma \mu_d}{\lambda_d + 2\mu_d} \\ 0 & -\omega^2 \rho & -ip_x & 0 & -\omega^2 \rho_f & 0 \\ +ip_x \frac{\rho_f}{q} - 2ip_x \frac{\sigma \mu_d}{\lambda_d + 2\mu_d} & 0 & 0 & -\frac{\sigma^2}{\lambda_d + 2\mu_d} & 0 & \frac{p_x^2}{q\omega^2} - \frac{1}{M} - \frac{\sigma^2}{\lambda_d + 2\mu_d} \\ 0 & \omega^2 \rho_f & 0 & 0 & \omega^2 q & 0 \end{pmatrix} \quad (\text{A-1})$$

For the effective medium, we define typical combinations of the poroelastic constants with a tilde on top. They turn out to be the corresponding dry-layer constants

$$\begin{aligned} \tilde{B}_2^* &= B_2^* - \frac{B_6^{*2}}{B_8^*}, \\ \tilde{B}_3^* &= B_3^* - \frac{B_6^* B_7^*}{B_8^*}, \\ \tilde{B}_4^* &= B_4^* - \frac{B_7^{*2}}{B_8^*}. \end{aligned} \quad (\text{A-2})$$

The matrix $\underline{\mathbf{P}}^*$ then can be written as

$$\underline{\mathbf{P}}^* = \begin{pmatrix} 0 & -ip_x & \frac{1}{\tilde{B}_5^*} & 0 & 0 & 0 \\ -ip_x \frac{\tilde{B}_3^*}{\tilde{B}_4^*} & 0 & 0 & \frac{1}{\tilde{B}_4^*} & 0 & -\frac{B_7^*}{B_8^* \tilde{B}_4^*} \\ P_{31}^* & 0 & 0 & -ip_x \frac{\tilde{B}_3^*}{\tilde{B}_4^*} & 0 & P_{36}^* \\ 0 & -\omega^2 \rho^* & -ip_x & 0 & -\omega^2 \rho_f^* & 0 \\ P_{51}^* & 0 & \frac{B_7^*}{B_8^*} \frac{1}{\tilde{B}_4^*} & 0 & 0 & P_{56}^* \\ 0 & \omega^2 \rho_f^* & 0 & 0 & \omega^2 q_z^* & 0 \end{pmatrix} \quad (\text{A-3})$$

The missing elements of $\underline{\mathbf{P}}^*$ are

$$P_{31}^* = -\omega^2 \left(\rho^* - \frac{\rho_f^{*2}}{q_x^*} \right) + 4p_x^2 \left(2\tilde{B}_1^* + \tilde{B}_2^* - \frac{\tilde{B}_3^{*2}}{\tilde{B}_4^*} \right), \quad (\text{A-4})$$

$$P_{36}^* = -ip_x \frac{\rho_f^*}{q_{xy}^*} + ip_x \left(\frac{B_7^* \tilde{B}_3^*}{B_8^* \tilde{B}_4^*} - \frac{B_6^*}{B_8^*} \right), \quad (\text{A-5})$$

$$P_{51}^* = -P_{36}^*, \quad (\text{A-6})$$

$$P_{56}^* = \frac{p_x^2}{q_{xy}^* \omega^2} - \frac{1}{B_8^*} - \left(\frac{B_7^*}{B_8^*} \right)^2 \tilde{B}_4^*. \quad (\text{A-7})$$

To include vertically downward propagating *SH*-waves, τ_{yy} as a function of components of the vector ζ is given for the layers as

$$\begin{aligned} \tau_{yy} &= \left(2ip_x \frac{\lambda_d \mu_d}{\lambda_d + 2\mu_d} \right) u_x + \left(\frac{\lambda_d}{\lambda_d + 2\mu_d} \right) \tau_{zz} \\ &\quad - \left(2 \frac{\sigma \mu_d}{\lambda_d + 2\mu_d} \right) p_f \end{aligned} \quad (\text{A-8})$$

and, accordingly, for the TIV effective medium as

$$\tau_{yy} = \left(ip_x \tilde{B}_2^* - \frac{\tilde{B}_3^{*2}}{\tilde{B}_4^*} \right) u_x + \left(\frac{\tilde{B}_3^*}{\tilde{B}_4^*} \right) \tau_{zz} - \left(\frac{B_7^* \tilde{B}_3^*}{B_8^* \tilde{B}_4^*} - \frac{B_6^*}{B_8^*} \right) p_f. \quad (\text{A-9})$$

In the next step, the matrix $\underline{\mathbf{P}}$ is averaged and each element is compared with the corresponding one for the matrix $\underline{\mathbf{P}}^*$. The coefficients of equations (9) and (10) are treated in the same way. This results (using only terms of the lowest order in frequency) in 10 equations that must be solved for the eight effective poroelastic constants and q_{xy}^*, q_z^* . As a simple example, consider the relation $\langle P_{2A} \rangle = P_{2A}^*$, which yields $\langle 1/(\lambda_d + 2\mu_d) \rangle = 1/\tilde{B}_4^*$, which is one of the results given in equation (14).